# The hysteretic response of a shallow pyroclastic deposit

Luca Comegna[1], Emilia Damiano[1], Roberto Greco[1], Lucio Olivares[1], Luciano Picarelli[2]

[1]Department of Engineering, University of Campania "Luigi Vanvitelli", Aversa, 81031, Italy
[2]JTC1 "Natural Slopes and Landslides", Chair, Federation of International Geo-Engineering Societies (FedIGS), Naples, 80131, Italy

*Correspondence to*: Luca Comegna (luca.comegna@unicampania.it)

**Abstract.** The paper reports field data provided by the automatic monitoring of the annual hydrological response of a shallow deposit of loose pyroclastic soils located in a mountainous area of Campania, Southern Italy. The monitoring station is installed along the northern slope of mount Cornito, about 2 km east of the town of Cervinara, which in December 1999 had been involved in a rainfall-induced flowslide. The collected data concern rainfall height, soil moisture content and suction. In particular, the installation at the same depths of suction and moisture sensors allows to estimate the soil water retention features that seem to indicate some hysteretic nature of the wetting/drying processes induced by weather conditions and their influence on the local stability conditions.

The data reported in the paper are freely available at https://doi.org/10.5281/zenodo.4281166 (Comegna et al., 2020).

## 1 Introduction

The hydraulic response of unsaturated soils subjected to infiltration and/or evaporation phenomena is usually modelled through the well-known *Soil Water Retention Curve*, SWRC, correlating matric suction, $s$, with volumetric water content, $\theta$. Experimental evidence and theoretical considerations (Mualem, 1976; Pham, 2002; Wheeler et al., 2003; Tami et al., 2004; Li, 2005; Tarantino, 2009; Yang et al., 2012; Pirone et al., 2014; Comegna et al., 2016c; Chen et al., 2017; Chen et al., 2019; Rianna et al., 2019) indicate that the SWRC is not univocal, but may depend on soil initial conditions and on the induced wetting or drying paths, revealing an hysteretic nature.

Figure 1 shows the typical response of an initially saturated soil specimen subjected to drying and wetting cycles. During the first drying stage, the volumetric water content decreases from the initial value, $\theta_{s,d}$, following a path, known as the *main drying curve*, until attaining the minimum, corresponding to a high suction value, known as the "residual soil moisture content", $\theta_r$. In the subsequent wetting process the volumetric water content increases along a different path, known as the *main wetting curve* (Fig. 1), until reaching a final maximum value, $\theta_{s,w}$, at zero suction: $\theta_{s,w}$ is usually different from $\theta_{s,d}$ because of some air entrapment that prevents to reach a saturation degree equal to one. However, in some cases, if the wetting process is very slow, it may occur that $\theta_{s,w} \cong \theta_{s,d}$.

If moving along one of these paths a reverse process is initiated, the main path is abandoned and a different *scanning curve*, located between the two main paths, is then travelled (Fig. 1). Scanning curves, which in turn may be characterised by

internal hysteretic loops, present a lower slope than the main curves: this physically means that, starting from the same matric suction, the variation in soil moisture corresponding to a given suction change is smaller running a scanning than a main curve. As shown in Figure 1, the final part of a scanning path may coincide with the nearest primary curve. Concerning this point, Tami et al. (2004) report the results of some tests carried out on a 30° model slope consisting of a 40 cm thick

35 layer of fine sands, overlying a 20 cm thick layer of gravelly sands, subjected to artificial precipitations of different intensity. Figure 2 shows the scanning curves obtained by fitting the coupled data measured by a tensiometer and a TDR located at a depth of 30 cm during two consecutive drying stages (1-2, 2-3) and two consecutive wetting stages (4-5, 5-6). The main drying and wetting curves had been independently obtained through a Tempe cell and capillary rise tests.
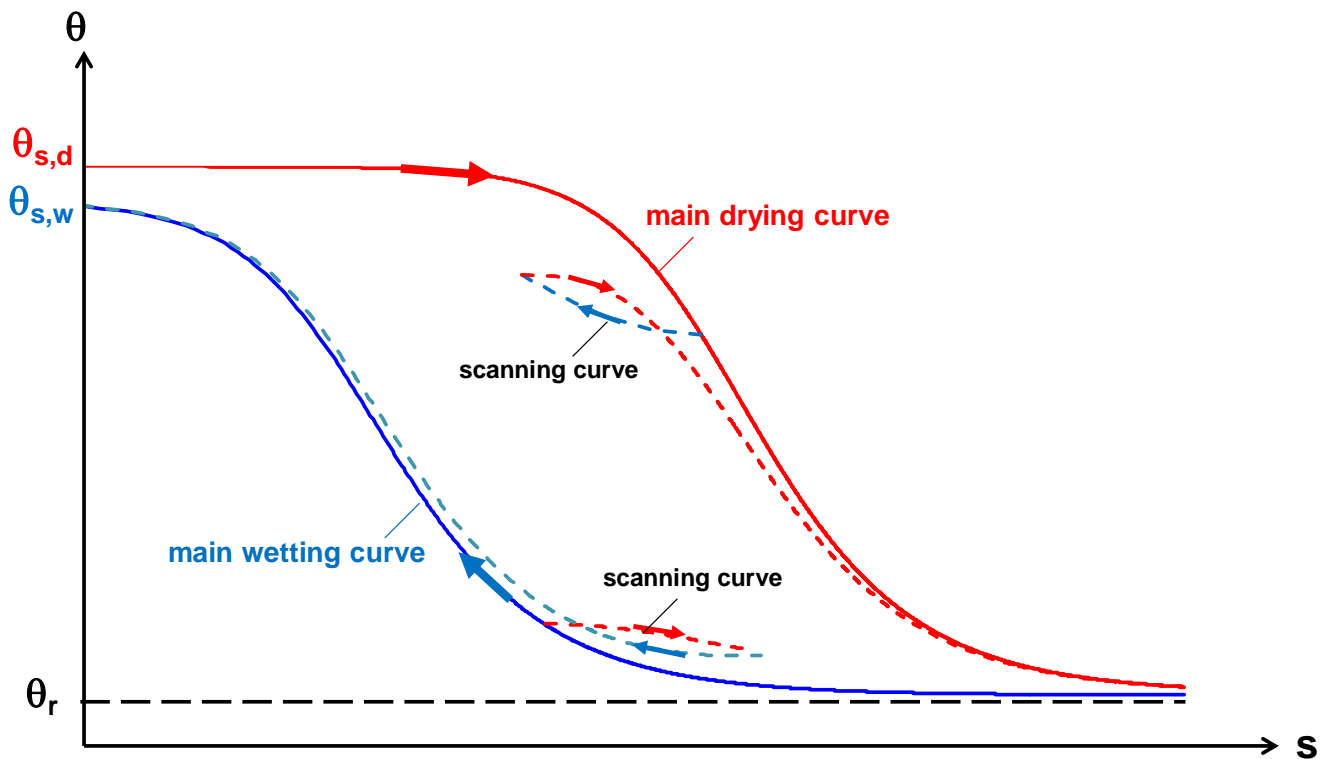
40 **Figure 1: Hysteretic wetting/drying paths.**
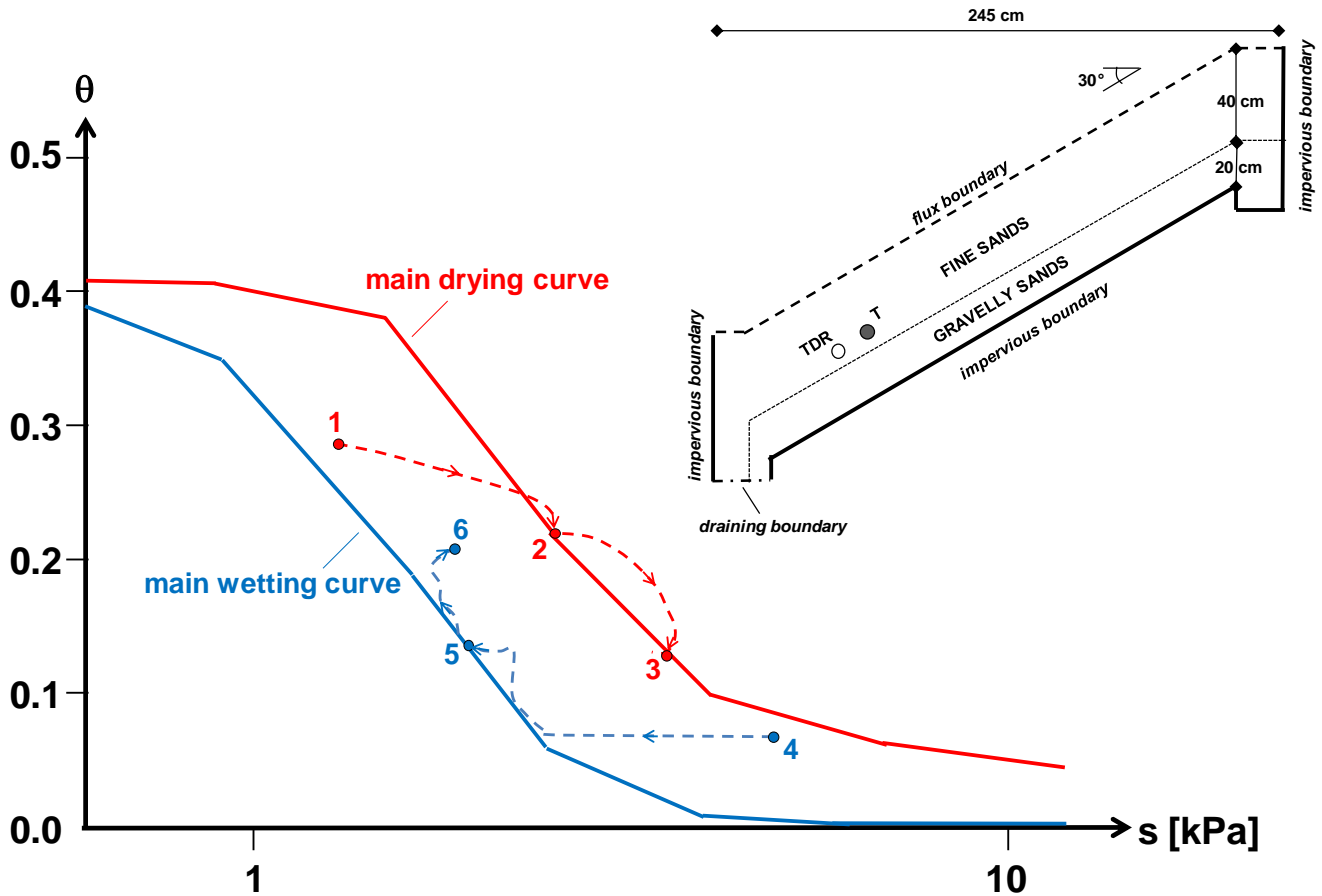
**Figure 2: Scanning curves obtained from flume tests carried out by Tami et al. (2004).**

45

The described hydraulic soil response, known as *hydraulic hysteresis*, may be related to microscopic phenomena affecting the energy state of water at pore scale (i.e. variations of contact angle during solid particles wetting and drying, or bottlenecks differently affecting filling and emptying of pores), as well as macroscopic phenomena depending on the boundary conditions and on the rate of the specific transient wetting/drying process (e.g. air entrapment). Consequently, the

50  same water content may be associated with different water potential energies, thus with different suction values within an interval defined by the highest and lowest limits respectively imposed by the main drying curve and the main wetting curve.

Field monitoring is doubtless a helpful tool to fully understand the hydrological behaviour of soils. Well aware that such response could in turn affect the stability conditions of the slope, an automatic monitoring station has been installed in a shallow layer of loose pyroclastic soils covering a steep mountainous area in a site in Campania Region (Southern Italy),

55  which in 1999 had been the seat of rainfall-induced flowslide causing the death of four people (Olivares and Picarelli, 2003). The availability of continuous data, consisting of rainfall height, soil moisture content and suction readings, allowed to

collect useful information. The data reported in the present paper concern the time period going from January, 2011, to January, 2012. Such data have been also used to estimate the slope stability conditions at the investigated depths.

## 2 Monitoring site

60  The site is located at an elevation of 560 m a.s.l., on the North-East facing slope of mount Cornito (Fig. 3a), 2 km far from the town of Cervinara (Campania Region, Southern Italy). The area is characterised by a humid Mediterranean climate, with most precipitations occurring between October and April and warm and dry summer. The mean annual rainfall height is around 1600 mm, and the mean annual potential evapotranspiration around 750 mm (Marino et al., 2020). Figure 4 reports mean monthly values of rainfall height, mean daily temperature and evapotranspiration.

65
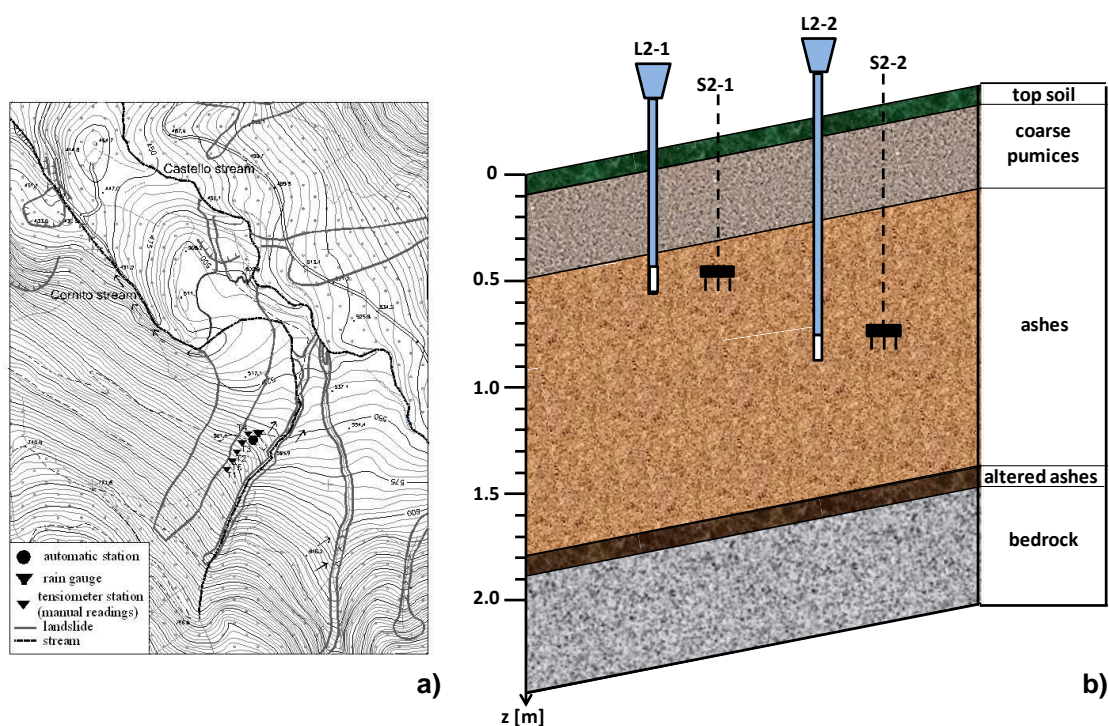
**Figure 3: Location of the automatic monitoring station (modified after Damiano, 2004) (a), and sketch of the local stratigraphy and position of the sensors (b).**

70
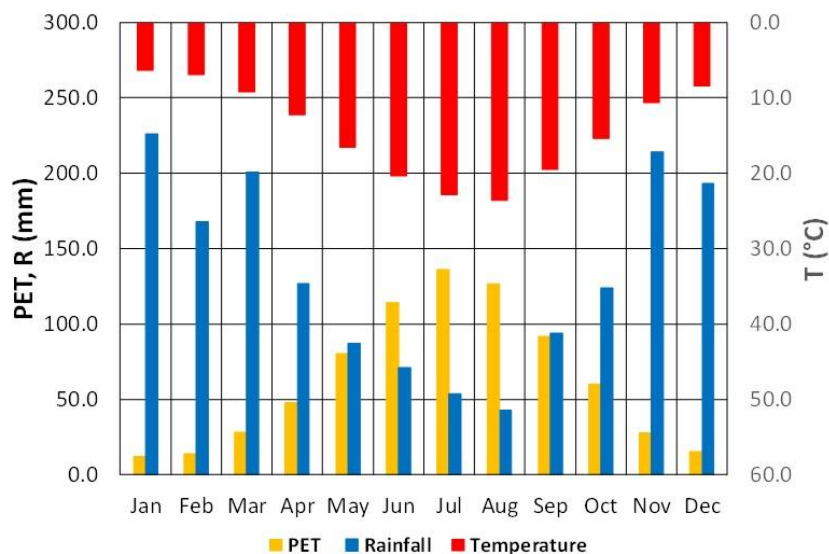
**Figure 4: Mean monthly values of rainfall height, R, temperature, T, and potential evapotranspiration, PET, estimated with the Thornthwaite expression (1946).**

75  Geological surveys and geotechnical investigations reveal that the basal Mesozoic–Cenozoic fractured limestones are overlain by air-fall sandy soils resulting from the explosive volcanic activity of Somma–Vesuvius and Phleagraean Fields (Fiorillo et al., 2001; Picarelli et al., 2006; Damiano et al., 2012). In particular, the pyroclastic deposits consist of alternating layers of ashes and pumices, more or less parallel to the bedrock surface, with a thickness strongly dependent on the slope angle, ranging from some decimetres in the steepest upslope zones (about 50°) to more than 10 m at the foot of the hill

80  (Guadagno et al., 2011). Some layers locally miss, possibly as a result of past landslides or of erosive processes. Cultivated chestnut trees are widespread on the slope, except some areas where the vegetation consists of shrubs and grass. When the tree foliage is present, usually from May to late September, a dense underbrush grows, mainly formed by ferns and other seasonal shrubs. Differently, in October the leaves get dry and fall, and the underbrush disappears until the following late spring. During late autumn and winter the ground is mostly covered by a layer of litter, mainly originating from fallen

85  chestnut leaves. The seasonal variations of vegetation affect the soil hydrologic response to meteorological forcing by: i) interception of the precipitation caused by canopy, understory and litter; ii) root water uptake, that distributes the total evapotranspiration flux over the root depth, according to the local value of soil water potential, which is highly variable throughout the year owing to the dormant leafless vegetation in winter (Comegna et al., 2013). Visual inspections in trenches dug during the investigations that have been carried out on site showed that roots usually extend across the entire soil depth

90  up the basal limestones, with a maximum density within the uppermost 0.50 m of soil cover, becoming sparse below the depth of 1.50 m.

The monitored deposit is 1.9 m thick with a sloping angle of about 40°. The local stratigraphy consists of the following unsaturated soil layers (Fig. 3b): 1) topsoil, 10 cm thick; 2) coarse pumices, 40 cm thick; 3) ashes, 1.30 m thick; 4) altered ashes, 10 cm thick, located just above the bedrock. The volcanic ash is a sandy silt, the pumices are sandy gravels. The

95    lowermost thin altered ash layer overlying the bedrock is a sandy silt with a plasticity index ranging in the interval 10–30%. The soil porosity ranges between 50% and 75% (Table 1). The shear strength parameters are typical of essentially cohesionless coarse grains soils.

**Table 1: Main physical properties of the pyroclastic cover.**

| layer | $\gamma_s$ [kN/m$^3$] | $\gamma$ [kN/m$^3$] | porosity [%] | c'[kPa] | φ'[°] |
|---|---|---|---|---|---|
| coarse pumices | 23 | 13 | 50-55 | 0 | 45 |
| ashes | 26 | 14 | 68-75 | 0 | 38 |
| altered ashes | 26 | 16 | 60 | 2 | 38 |

100

Monitoring started at the beginning of 2002 (Olivares et al., 2003; Damiano et al., 2012). Rainfall was automatically recorded at a hourly time step by a rain gauge having a sensitivity of 0.2 mm. Soil suction was manually measured by "Jet-fill" tensiometers equipped with a Bourdon manometer, installed at different depths in the ash layers. An additional automatic monitoring station has been installed in 2009. It consists of eight "Jet-fill" tensiometer, equipped with tension

105    transducers, and of seven metallic probes for Time Domain Reflectometry (TDR) aimed at measuring volumetric water content (Comegna et al. 2016a). The ceramic tips of the tensiometers were pushed into the soil through small holes previously dug by a drill. The uppermost part of the hole was then filled with a bentonite–cement mixture to avoid any water infiltration. A careful maintenance was granted by regularly checking the complete saturation of the instruments (especially after long-lasting dry periods) and filling the tube with de-aired water in order to remove air bubbles; moreover, the

110    instruments were carefully checked after cold periods when low temperatures could freeze. The soil moisture sensors consist of three 100-400 mm long metallic rods having a diameter of 3 mm and spacing of 15 mm. Once vertically buried in the soil, the probes were connected through coaxial cables and a multiplexer to a Campbell Scientific Inc. TDR-100 reflectometer. TDR readings provide the soil bulk dielectric permittivity, $\varepsilon_r$, which can be converted to soil volumetric water content, θ, through a calibration relationship (Topp et al., 1980). A specific relationship has been purposely found by Guida et al. (2012)

115    through targeted laboratory tests on undisturbed samples taken nearby the monitoring station; the average error in the estimation of the volumetric water content is ±0.02 m$^3$/m$^3$. All the sensors are connected to the Campbell Data Logger. The monitoring station is powered by a solar panel with a 12V backup battery. The automatic acquisition and storage of data is set with a time resolution of six hours.

The following section describes the field data collected from January, 1$^{st}$, 2011 to January, 31$^{st}$, 2012 at the depths z = 0.60

120    m and z = 1.00 m, where the 7 cm long tensiometer ceramic tips, L2-1 and L2-2, are located in the ash layer in vicinity of the 40 cm long TDR probes S2-1 and S2-2 (Fig. 3b). For the sake of clarity, it has to be pointed out the sensors sample different soil volumes; this might lead to an imperfect matching of data.

Regarding the water retention properties, Figure 5 shows the results of nine laboratory wetting tests performed by Damiano and Olivares (2010) and by Olivares et al (2019). Such tests were carried out in the laboratory on a 40 cm thick model slope
125 formed with Cervinara ash and volcanic ashes with same grain size taken from the nearby Monteforte Irpino sloping site. The model slope was reconstituted at the field porosity of 75%. During artificial infiltration tests, soil matric suction and moisture content were respectively measured by a miniaturised tensiometer and a TDR probe installed close to each other at depths from 1.5 to 8.5 cm. The initial soil moisture and suction values were respectively in the range 0.21-0.34 and 15-60 kPa (Fig. 5). The wetting curve first ran rather a flat wetting path and then a steeper path until attaining full saturation. The
130 experimental points along such a steepest curve were fitted with the van Genuchten equation (1980)

$$\vartheta = \vartheta_r + \frac{\vartheta_s - \vartheta_r}{[1+(\alpha s)^n]^m} \qquad (1),$$

assuming $\theta_s = 0.75$ (that corresponds to the soil porosity) and $\theta_r = 0$ (a value which is consistent with the coarse-grained nature of the soil), Table 2 shows the best fitting $\alpha$, $n$ and $m$ values. In order to help the interpretation of the in-situ hydrological response, the obtained curve is reported in the next section, together with the monitored field data as a possible
135 reference lowest boundary.
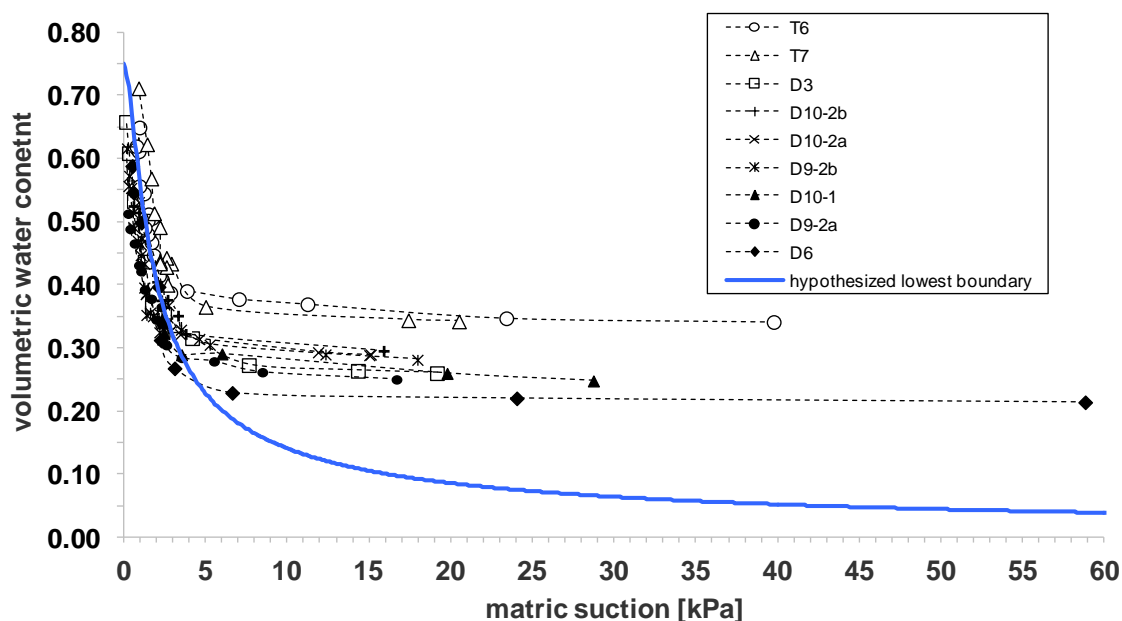
**Figure 5: Coupled values of matric suction and water content measured during infiltration tests (Damiano and Olivares, 2010, and Olivares et al., 2019).**

140 **Table 2: Van Genuchten parameters (Eq. 1), representative of the lowest water retention boundary shown in Figure 5.**

| $q_s$ | $q_r$ | $\alpha$ [kPa$^{-1}$] | $n$ | $m$ |
|-------|-------|----------------------|------|------|
| 0.75 | 0.00 | 1.00 | 1.72 | 0.42 |

# 3 Results of field monitoring

The wetting and drying processes affecting the cover are of course strictly governed by the weather forcing, typical of the Mediterranean climate, characterized by warm and dry summer. Figure 6 shows the monthly cumulative precipitations in 2011 provided by the rain gauge installed on the slope, and the average monthly values of minimum, $T_{min}$, daily mean, $T_{med}$,

145 and maximum, $T_{max}$, temperature monitored by a local weather station managed by Campania Civil Protection Agency. The total cumulative rainfall was 1360 mm, a value lower than the mean yearly rainfall in the same area. A daily precipitation higher than 1 mm was recorded 99 times; the daily rainfall exceeded the value of 50 mm only in five cases (February, 16th; April, 30th; September, 19th; November, 6th; December, 5th). March was the rainiest month, with a total precipitation of 296 mm, i.e. 22% of the yearly rainfall. The dry season started in June continuing until the end of October. In such a season some

150 significant isolated rainy events characterised by daily precipitations ranging between 17.4 mm and 19.2 mm occurred on July, 29th; September, 7th; October, 8th; October, 22nd; another more severe event totaling 53 mm took place on September, 19th. In November and December the cumulative rainfall was about 30% of the annual precipitation: the most intense daily rainfall occurred on November, 6th (58 mm).

The daily mean air temperature was close to average, with a slightly warmer summer. The potential evapotranspiration can

155 hence be assumed to be close to the average estimated values shown in Figure 4. In particular, the mean daily temperature was higher than 15°C from May, 19th, to October, 7th, attaining values higher than 20°C from July, 30th, to September, 18th. The lowest $T_{min}$ value was measured in February (4 °C), and the highest $T_{max}$ (31 °C) in August.

The data obtained by coupling moisture content and matric suction at the depths of 0.60 m and 1.00 m are discussed in the following section by distinguishing eight time windows characterized by different weather conditions. Due to some technical

160 problems, related to the emptying of the tensiometers (occurring especially during the warmest periods) or to some loss in battery power, the records present some data lacks. In particular, unfortunately no retention data are available from July, 19th to November, 4th, 2011 and from December, 6th, 2011 to January, 6th, 2012.
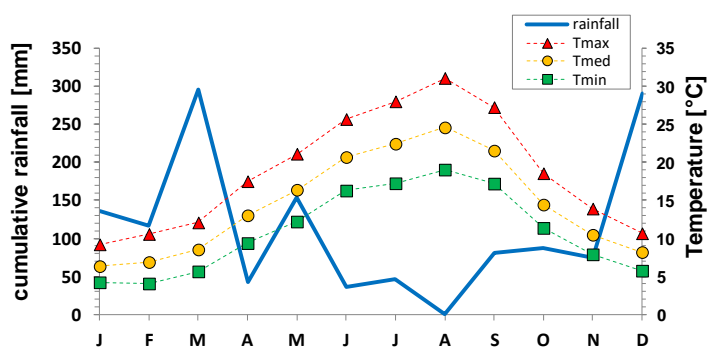
165 **Figure 6: Monthly cumulative rainfall and average monthly minimum ($T_{min}$), daily mean ($T_{med}$) and maximum ($T_{max}$) values of air temperature monitored in 2011.**

### 3.1 Time window A-B: January, 1st - May, 8th 2011

The total precipitation in this time interval was 695 mm, which corresponds to 51% of the annual cumulative value. Until March, 12th, the mean daily air temperature ranges between 0.5°C and 12.8°C (Fig. 7a), then it steadily increases from 5.8°C to 16.7°C (with an increasing trend of 1.8°C/month).

On January, 1st, the moisture content and matric suction measured by S2-1 and L2-1 at depth of 0.60 m are respectively 0.39 and 11 kPa (Fig. 7b). Such values are the result of the antecedent weather conditions; in particular, the total precipitation in the previous 30 days had been 170 mm and the mean daily air temperature 7°C (Fig. 7a). As shown in Figure 7b, the soil moisture content measured in the examined window is 0.34-0.41 while the matric suction ranges in the interval 3-16 kPa. During the dry days, the soil moisture decreases with a rate of -1%/month while suction tends to increase with an average rate of about 1.4 kPa/month. Such a drying path is periodically reversed by some rainfall-induced wetting processes. In particular, three sudden drops of suction are recorded on January, 23rd, February, 17th, and May, 1st, due to very similar rainfall events featured by a total precipitation of 48-58 mm cumulated over the antecedent 48 hours.

At depth of 1.00 m, the volumetric water content, measured by S2-2, and suction, measured by L2-2, range respectively in the intervals 0.29-0.37 and 4-16 kPa (Fig. 7c). Soil moisture tends to decrease of -0.8%/month, while suction is increasing with an average rate of about 1.0 kPa/month. Such trends are hence slower than at the shallower depth. This reflects a minor role of evapotranspiration during winter and early spring (when the vegetation is leafless), when the soil profile is slowly drained downward owing to the existing small water potential gradient, which departs from the gravitational -1 only during rainfall. The large amount of precipitation and the small variations of water content and soil suction at both depths suggest that the soil cover is being crossed by an intense downward flux, which causes temporary small increments of water content in response to rainfall events, followed by slower reductions. Indeed, at both depths the water content is steadily higher than the field capacity (i.e. about 0.25 m³/m³).

All data have been reported in the water retention plane s-θ, shown in Figure 8a and 8b, together with the corresponding fitting curves, named AB. At both investigated depths, the fitting curve AB is quite flat with an overall slope of about -0.4 %/kPa.

### 3.2 Time window B-C: May, 8th - June, 22nd 2011

This window is featured by a cumulative rainfall of 85 mm and a daily air temperature ranging in the interval 10-24°C, with an increasing trend of 4.3°C/month (Fig. 7a). During this season, vegetation starts growing further and further thus accommodating the increasing evapotranspiration demand and influencing the hydrological soil response through root water uptake.

At depth z = 0.60 m, suction ranges between 10 kPa and 24 kPa, growing with a rate of about 9 kPa/month. This matches a reduction in soil moisture, that reaches the value of 0.25 with a decreasing trend of -9 %/month (Fig. 7b), which is more pronounced than during the previous time window due to an intense root water uptake from the uppermost soil layer.

200 Collected data can be well fitted by the curve BC in Figure 8a provided by Eq. (1) through the parameters shown in Table 3 (using again $\theta_s = 0.75$ and $\theta_r = 0$). The path BC is clearly steeper than the curve AB.

**Table 3: Van Genuchten parameters (Eq. 1) representative of the curve BCD curve shown by Figure 8a.**

| $q_s$ | $q_r$ | $\alpha$ [kPa$^{-1}$] | $n$ | $m$ |
|-------|-------|----------|------|------|
| 0.75 | 0.00 | 0.11 | 2.17 | 0.54 |

205 At depth z = 1.00 m (Fig. 7c), until June, 6th, water content and suction display little variations, moving respectively from 0.33 to 0.31 and from 15 kPa to 17 kPa. Measured values are again well fitted by the curve AB (Fig. 8b). After such a period, which is probably still characterized by some gravitational downward drainage, the soil starts drying quickly at this depth too being forced by root water uptake. The water content decreases with a rate of about -4%/month attaining a value of 0.27 at the end of this time window, while the increasing suction rate is similar to the one observed at 0.60 m. Such data are

210 well interpolated by the path CD (Fig. 8b), which is steeper than the path AB, but gentler than the CD curve detected at 0.60 m because of a lower evapotranspiration effect. The fitting parameters, reported in Table 4, are different from those obtained for z = 0.60 m (Table 3). Besides to evapotranspiration effects, such differences might be justified also by small differences in grain size and/or void ratio of the soil (Comegna et al., 2016a).

215

**Table 4: Van Genuchten parameters (Eq. 1) representative of the curve CD shown by Figure 8b.**

| $q_s$ | $q_r$ | $\alpha$ [kPa$^{-1}$] | $n$ | $m$ |
|-------|-------|----------|------|------|
| 0.75 | 0.00 | 0.76 | 1.33 | 0.25 |
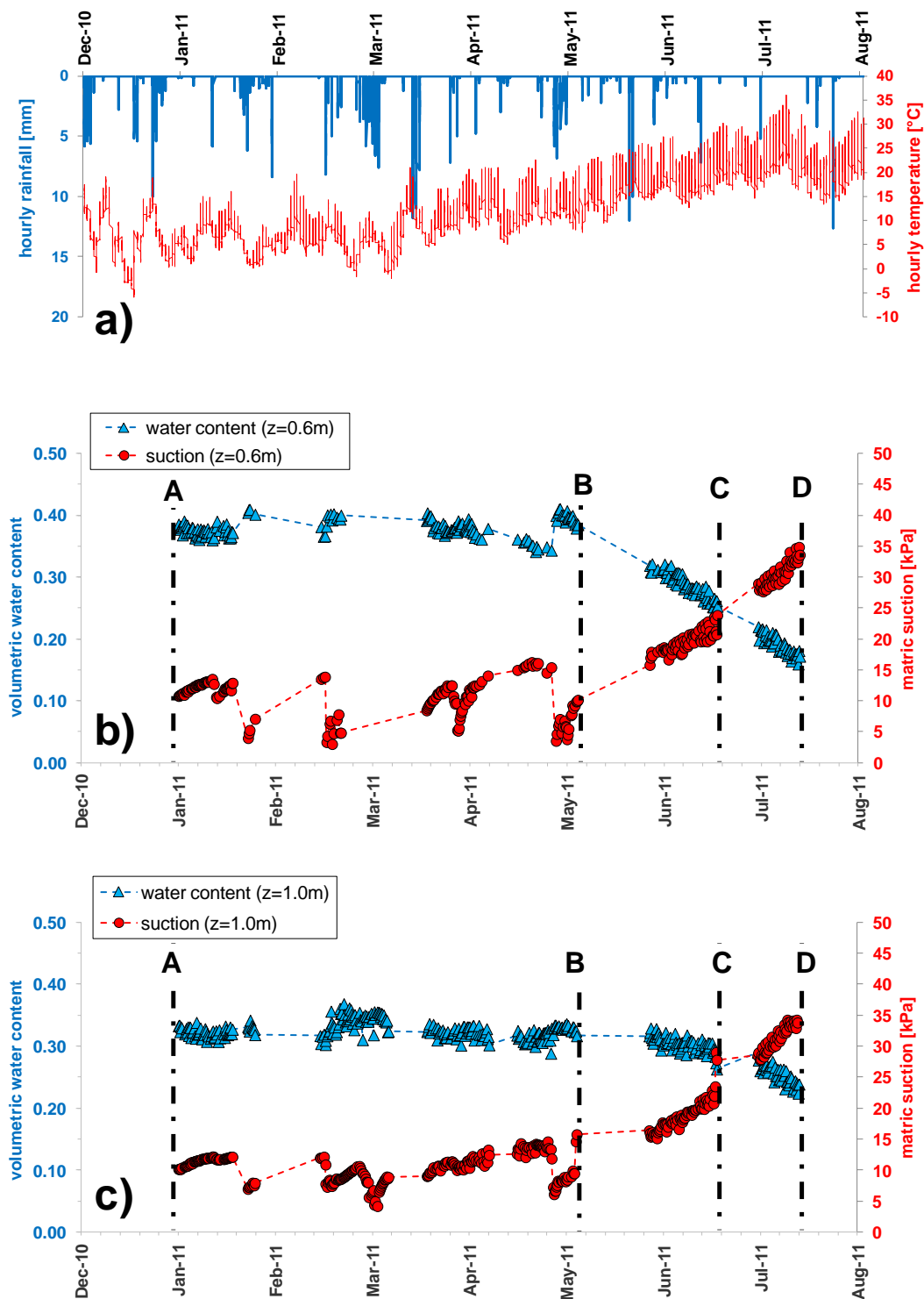
**Figure 7: Hourly weather data (a), matric suction and volumetric water content monitored from January to July, 2011 at depth z = 0.60 m (b) and z = 1.00 (c).**
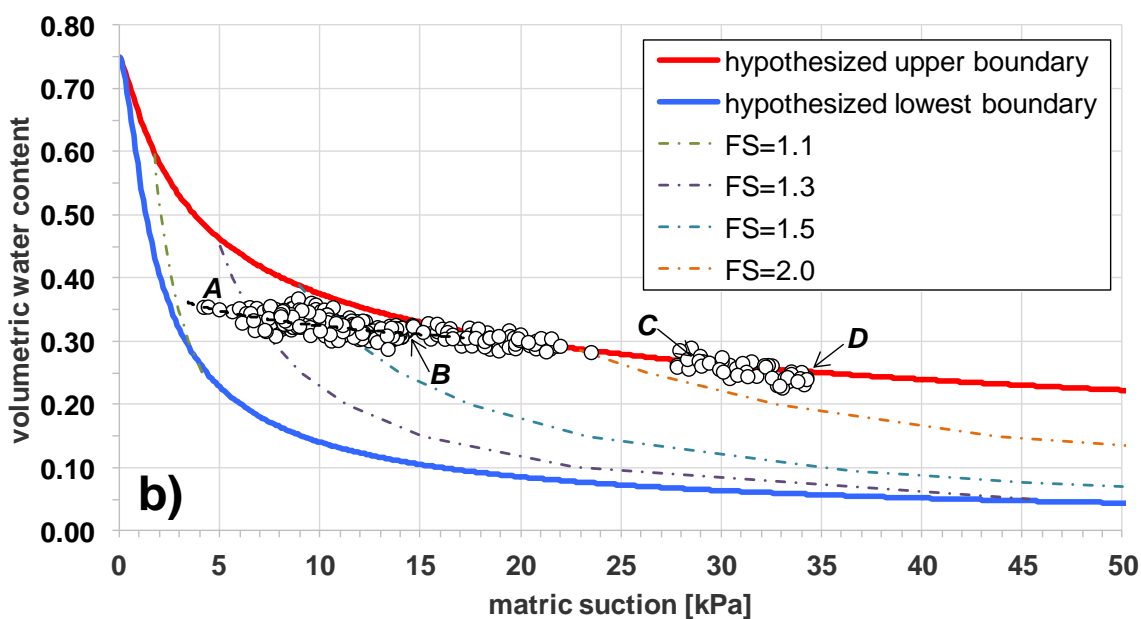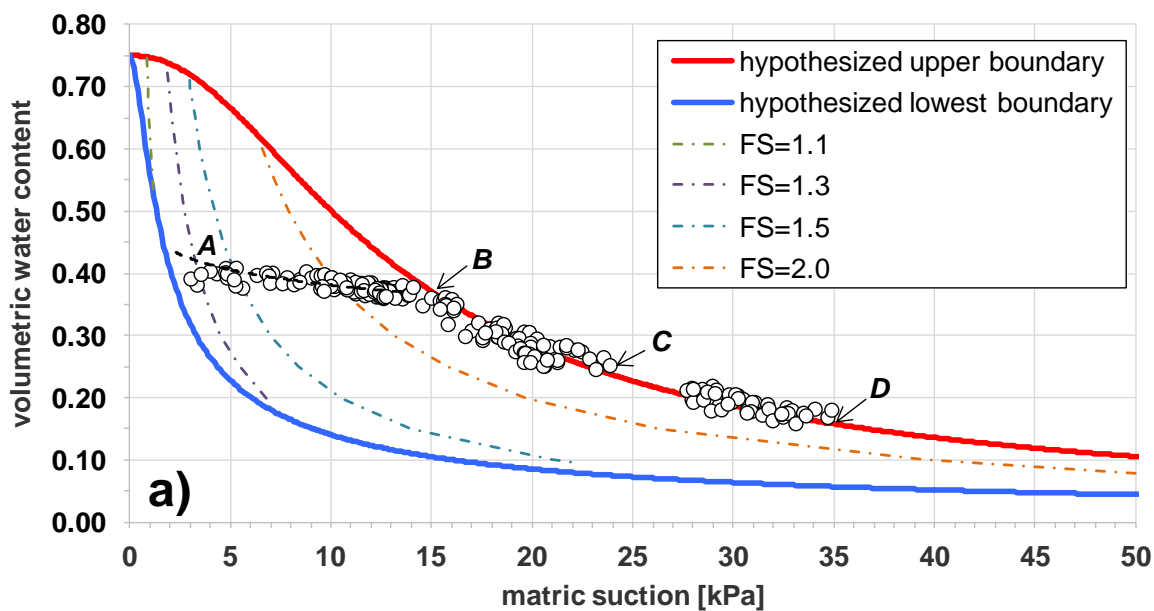
220

**Figure 8: Volumetric water content and matric suction recorded from January to July, 2011 at depths z = 0.60 m (a) and z = 1.00 m (b) and iso-Safety Factor curves.**

### 3.3 Time window C-D: June, 22$^{nd}$ - July, 18$^{th}$ 2011

225   In such a dry time interval the average daily temperature is 23.7°C with an increasing trend of 3.3°C/month and the cumulative rainfall is 14 mm (Fig. 7a). The flourishing vegetation and the high temperature suggest that evapotranspiration is largely exceeding infiltration by rainwater causing drainage of the soil cover owing to the action of plant roots.

At z = 0.60 m, the soil moisture reaches a value of 0.17, while suction grows by about 22 kPa/month until a value of 35 kPa (Fig. 7b). It is worth noting that in the retention plane the path BC can properly fit recorded field data (Fig. 8a).

230   At z = 1.0 m, soil moisture reaches the value of 0.24, while suction increases with a rate of about 13 kPa/month attaining a value of 34 kPa (Fig. 7c). In the retention plane, the field data are well interpolated by the curve CD (Fig. 8b).

### 3.4 Time window E-F: November, 5$^{th}$ - November, 6$^{th}$ 2011

In the time interval from July, 19$^{th}$ to November, 4$^{th}$, during which, as already stated, monitoring of water content and suction stops, the air temperature goes from the mean value of 24.6°C, reached in August, to 14.4°C, in October. Regarding

235   precipitations, from September to October the rain gauge records a cumulative precipitation of 168 mm fallen in only 9 isolated rainy days (Fig. 9a). Such a few concentrated precipitations seem to have been recorded by the shallowest sensors only. In fact, if the data acquired on November, 5$^{th}$, are compared to those monitored on July, 18$^{th}$, we can notice a moisture increase (from 0.17 to 0.24) and a suction decrease (from 35 to 22 kPa) at 0.60 m (Fig. 9b), while the sensors at z = 1.00 m (Fig. 9c) record a small water content decrease (from 0.24 to 0.23) and an increase of suction, from 34 to 47 kPa.

240   The most intense daily rainfall in 2011 takes place on November, 6$^{th}$. The total precipitation is 58 mm (Fig. 9a) and causes a volumetric water content increase from 0.24 to 0.43 (Fig. 9b) at 0.6 m, and from 0.23 to 0.27 at 1.0 m (Fig. 9c). At both depths the highest drop in suction is recorded; in fact, the decrease measured by L2-1 is from 22 kPa to 1.9 kPa (Fig. 9b) and the one recorded by L2-2 is from 47 kPa to 13 kPa (Fig. 9c). These data are represented in the water retention plane by the paths EF (Figs. 10a and 10b) well different from those ran in May and June. It's worth noting that at the shallowest depth,

245   the final point F reaches the curve obtained by interpolating the flume tests described in Section 2 (Fig. 5), which might be considered to be a reliable lowest boundary (the main wetting curve).
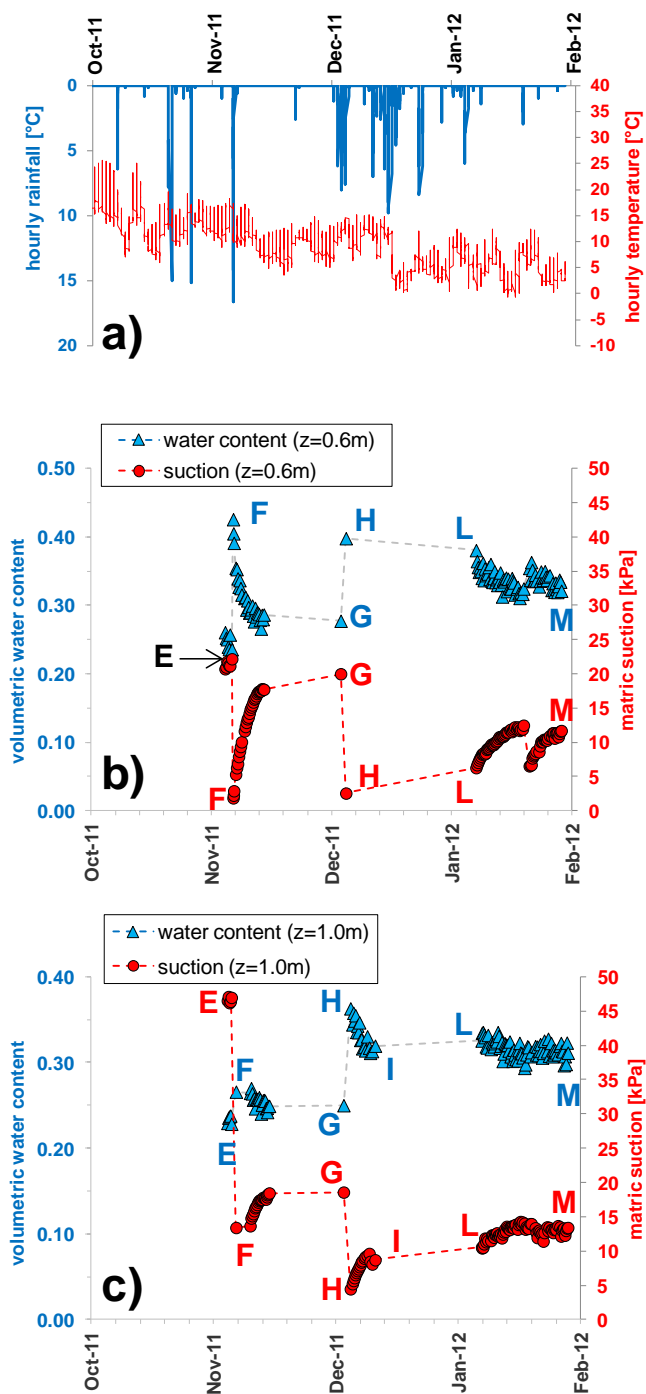
**Figure 9: Monitored hourly weather data (a), matric suction and volumetric water content from November, 2011 to January, 2012 at the depth z = 0.60 m (b) and z = 1.00 (c).**
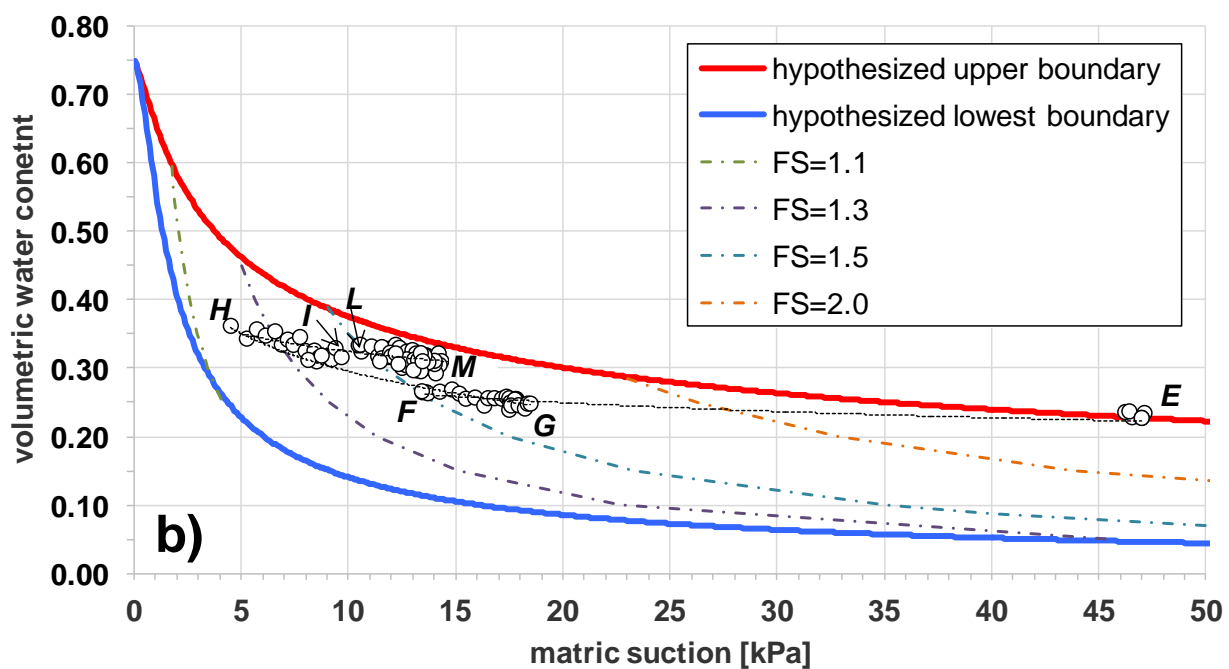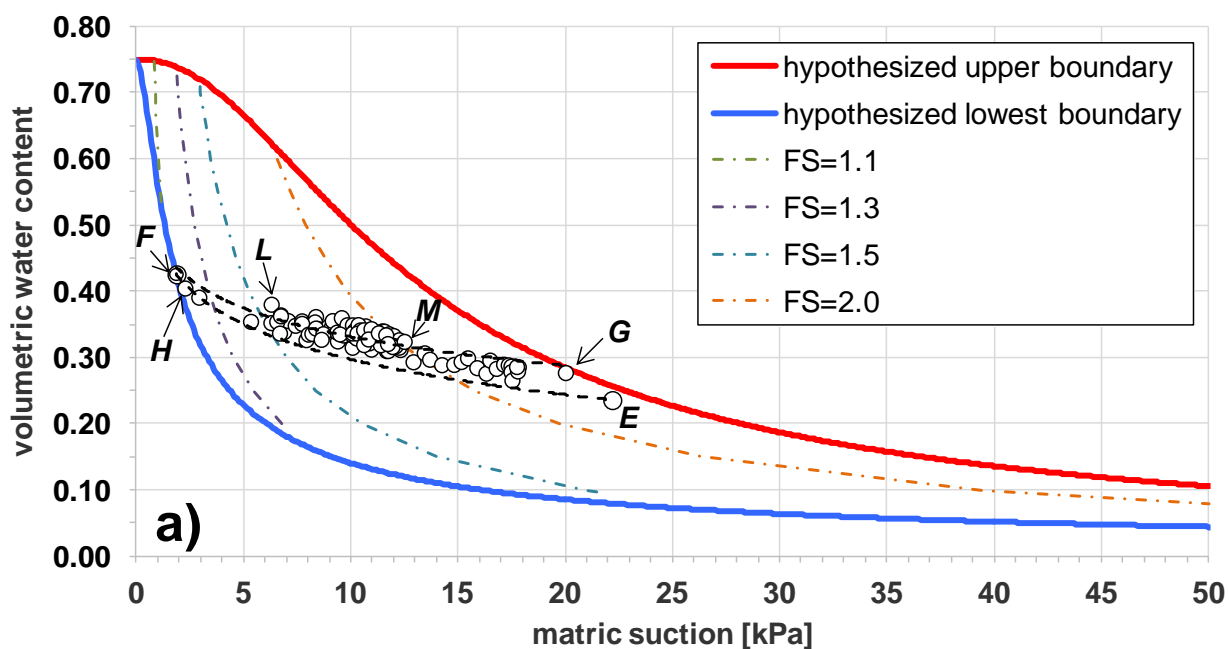
250

**Figure 10: Volumetric water content and matric suction, monitored from November, 2011 to January, 2012 at depths z = 0.60 m (a) and z = 1.00 m (b), and iso-Safety Factor curves.**

### 3.5 Time window F-G: November, 7th – December, 3rd 2011

Such a time interval is characterized by dry weather. In fact, one single rainfall event only of 12 mm occurs on November,
255  22n. The mean temperature is about 10°C. Moreover, leafless vegetation probably did not accommodate the small
evapotranspiration demand favouring an essentially downward flow, initially driven by a high potential gradient due to a
wetter uppermost soil profile, then progressively approaching a slow gravity driven drainage. In fact, at z = 0.60 m, the water
content decreases from 0.43 to 0.28 while soil suction increases from 1.9 kPa to 20 kPa (Fig. 9b). In the water retention
plane, the corresponding drying path FG is located above previous wetting path EF, about parallel to it (Fig. 10a). It is worth
260  to note that at point G it reaches the BCD curve travelled from May to July, confirming that drying develops according to
smoother paths and gently approaches the field capacity, when soil drainage is not forced by root water uptake.
At z = 1.00 m, the water content decreases from 0.27 to 0.25 and soil suction increases from 13 kPa to 19 kPa (Fig. 9c). The
corresponding drying path FG pursues backwards previous path EF (Fig. 10b).

### 265  3.6 Time window G-H: December, 5th 2011

On December, 5th, a single precipitation of 98 mm over 48 hours causes an increase of the water content at both depths. As a
consequence, at z = 0.60 m the water content grows from 0.28 to 0.40 and suction drops to 2.5 kPa  (Fig. 9b). The wetting
curve GH overlaps previous FG drying path (Fig. 10a). Again, the final point H reaches the assumed lowest boundary.
At z = 1.00 m the water content increases from 0.25 to 0.36, less than above, while suction decreases to 4.5 kPa. The final
270  point H does not reach the assumed main wetting curve (Fig. 10b).

### 3.7 Time window H-I: December, 6th – December, 11th 2011

No precipitations occur during this short time window.
Available data concern only depth z = 1.00 m. The moisture content decrease from 0.36 to 0.31 and soil suction increases to
275  10 kPa (Fig. 9c). The drying path HI is located above and parallel to the wetting path GH (Fig. 10b).

### 3.8 Time window L-M: January, 7th, 2011 – January, 31st, 2012

Such a period is characterized by negligible evapotranspiration owing to cold temperatures and leafless vegetation. Hence,
the observed trend of water content and suction can be ascribed to gravitational downward drainage, which in the long run
280  would lead the soil cover to approach field capacity.
Until January, 21st, 2012 suction increases from 6 kPa to 13 kPa at z = 0.60 m and from 10 kPa to 14 kPa at z = 1.00 m. On
that date, a 12-hours cumulative 16 mm rainfall causes a drop in suction of  6 kPa and 3 kPa respectively at the shallowest

and deepest tensiometers. Then suction increases again until the final values of 12 kPa (z = 0.60 m) and 13 kPa (z = 1.00 m) associated with water contents of 0.32 and 0.31.

285    All field data are quite well interpolated by the paths GH at z = 0.60 m (Fig. 10a) and HI at z = 1.00 m (Fig. 10b).

## 4 Discussion

The hydraulic paths plotted in Figs. 8 and 10 show that, at different times, different values of matric suction have been observed at both instrumented depths for the same the soil moisture content. The relationship between these two variables is then not univocal. In particular, the difference depends on the initial conditions (i.e. on the starting point). This reveals the

290    hysteretic nature of the hydrological soil response.

Therefore, all obtained paths should be considered as scanning curves located between the main drying and the main wetting curve. In more detail, the steepest drying paths obtained during the warmest days as a result of intense evapotranspiration owing to flourishing vegetation (curve BCD at z = 0.60 m; curve CD at z = 1.00 m) tend to the assumed main drying curve. It's also interesting to notice that, at 1.0 m depth, such final steeper path is reached on June, 6th, i.e. with a delay of about one

295    month with respect to the shallowest depth (where it has been attained on May, 8th). Such a result could be related to the delayed and mitigated effect of evapotranspiration due to the water uptake by roots, which are denser at depths less than 0.50 m, but are present down to a depth of 1.50 m more or less. During the periods of leafless vegetation and low temperatures, when the amount of evapotranspiration is modest, the drying paths are less steep and well below the assumed upper boundary.

300    All wetting paths move along gentler curves than the drying paths suggesting that vegetation does not affect soil wetting.

In order to estimate to what extent the slope stability conditions are affected by such a hysteretic response, some simple analyses have been carried out by the infinite slope model that is a suitable for Cervinara slope (Greco et al., 2013; Comegna et al., 2016b). In particular, assuming a homogeneous deposit with slope angle $\alpha = 40°$, unit weight $\gamma = 14$ kN/m$^3$, cohesion c' = 0, friction angle $\varphi' = 38°$, saturated volumetric water content $\theta_s = 0.75$, residual water content $\theta_r = 0$, the factor of safety

305    FS at depth z is provided by the formula:

$$FS = \frac{\tan\varphi'}{\tan\alpha} + \frac{c_{app}}{\gamma \cdot z \cdot \text{sen}\alpha \cdot \cos\alpha} \qquad (2)$$

where $c_{app} = s \cdot \frac{\vartheta - \vartheta_r}{\vartheta_s - \vartheta_r} \cdot \tan\varphi'$ is the expression provided by Vanapalli et al. (1996) to define the *apparent cohesion*, a

310    strength component which accounts for the role of suction. Assuming, $\gamma$ constant for the sake of simplicity, the variation of FS with time is only due to $c_{app}$ fluctuations. In particular, Eq. (2) shows that, at depth z = 0.60 m, slope stability is guaranteed by an apparent cohesion equal to or higher than 0.3 kPa, and by $c_{app}$ = 0.5 kPa or more at z = 1.00 m.

Figures 11 and 12 show the fluctuations of the safety factor FS during the period of monitoring . At z = 0.60 m, FS ranges between a minimum value of 1.13, attained on November, 6th (Fig. 12a), and a maximum of 2.22, on July, 5th (Fig. 11a),

315 which respectively correspond to $c_{app}$ values of 0.8 and 6.6 kPa. At z = 1.00 m, FS ranges between 1.18 and 2.60, on December, 5th, and on November, 5th (Fig. 12b), corresponding to a $c_{app}$ interval 1.5-11.6 kPa. The higher fluctuation of FS at the shallowest depth, z = 0.60 m is obviously due to a higher suction variation.

In Figures 8 and 10 the iso-Safety Factor curves, i.e. featured by constant FS values, have been plotted. At a given suction, $s$, FS increases with the soil moisture; this means that the lower scanning curves correspond to worse safety conditions. For

320 instance, looking at Figure 10, the FS values calculated along the wetting path EF, that originates after the dry season, are lower than those corresponding to the drying curve LM that starts after the rainfall events occurred in November and in December; also, the changing rate of the safety factor FS is always remarkable along the scanning paths where little changes of the soil moisture content can induce high suction changes.

It is interesting to notice that the lowest FS value is attained at z = 0.60 m on November, 6th, i.e. after the most intense

325 rainfall event recorded in 2011, when the wetting path reaches the assumed lower boundary at point F (Fig. 10a), featured by $s$ = 1.9 kPa and $\theta$ = 0.43. Starting from this condition, a further, just hypothetical, persistent and intense rainfall event could have forced the point to follow the final steeper branch of the main wetting curve, which has been obtained the flume tests (Fig. 5). In particular, the failure condition (FS = 1) would have been reached for a soil moisture $\theta$ = 0.69 ($s$ = 0.40 kPa), i.e. for a water content increase $\Delta\theta$ = 0.26 (or a suction decrease $\Delta s$ = -1.5 kPa). Such a large increase in the water content

330 indicates that landsliding in the area at hand is not so obvious, being the consequence of exceptional weather conditions as chronicles and statistical analyses suggest (Comegna et al., 2017).
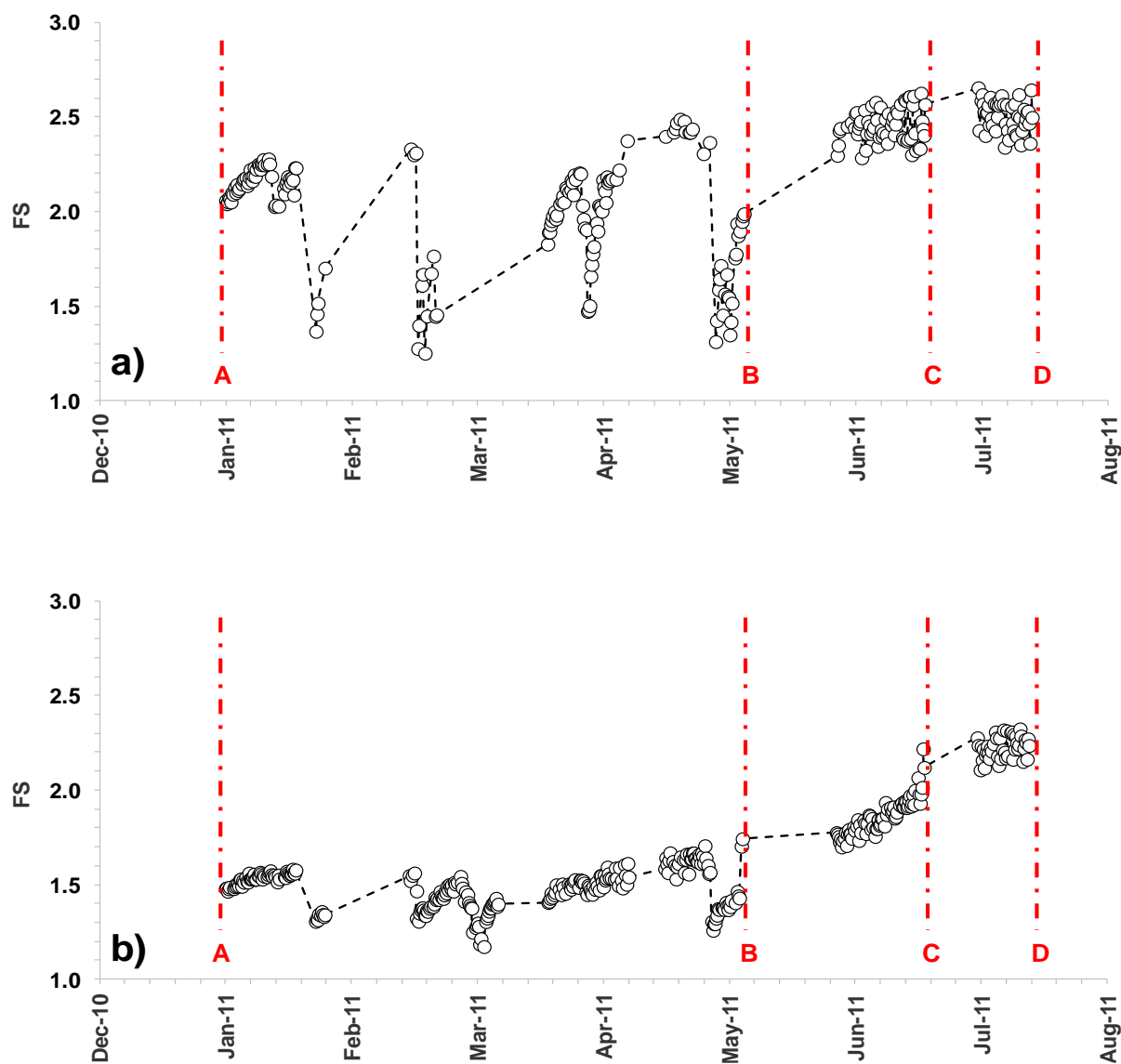
**Figure 11: Factor of Safety, FS, calculated from January to July, 2011 at the depth z = 0.60 m (a) and z = 1.00 m (b).**
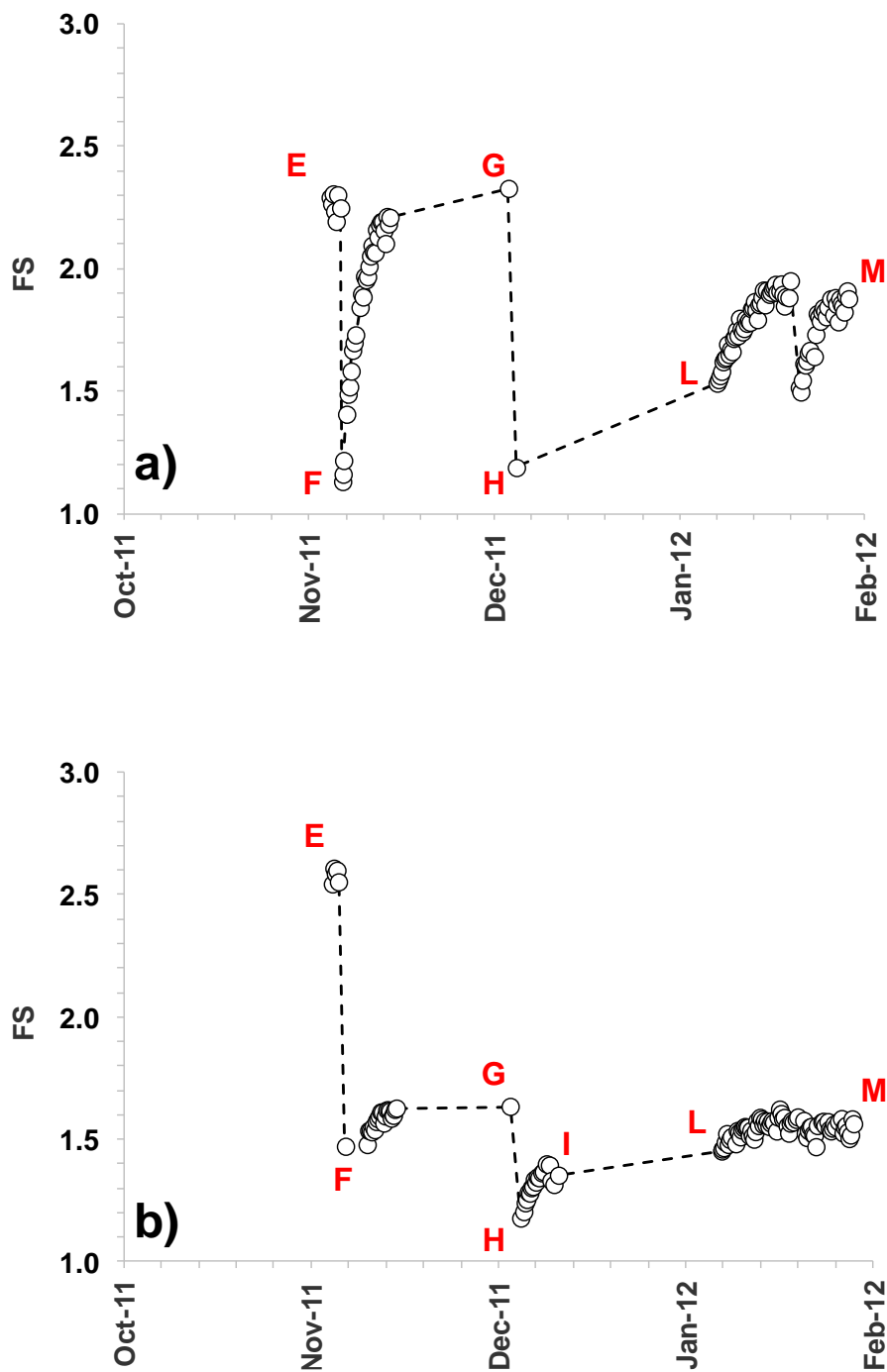
335

**Figure 12: Factor of Safety, FS, calculated from November, 2011 to January, 2012 at the depth z = 0.60 m (a) and z = 1.00 m (b).**

## 5 Conclusions

The setup of an automatic field station allowed monitoring the annual cyclic hydrological response of a sloping deposit in
340    pyroclastic air-fall soils. Even though the relationship between measured water contents and suction values has to be carefully considered accounting for all the factors which can adversely affect the validity of such a relationship (small differences in grain size or porosity, which is dependent also on the installation procedures of the soil around the sensors, different soil volumes affecting the response of sensors, different reliability in data interpretation), monitoring provide useful information about the hydrological soil response.

345    In particular, collected data highlight the influence of the initial conditions, which depend on the antecedent wetting/drying history, on the weather-induced hydraulic paths. In fact, different soil moisture values can be associated with the same matric suction due to the hysteretic soil response. Moreover, soil drying may be affected by evapotranspiration due to water exctraction by roots, and this in a different way in the different seasons.

As indicated by simple stability analyses, in the examined period the slope has been always quite far from failure conditions.
350    In particular, the hydraulic path leading to slope failure is generally featured by quite a high soil moisture change. This is well detectable by TDR sensors, but is characterized by so low suction changes (less than 2 kPa) to be hardly measurable by ordinary tensiometers. Such results unavoidably raise some questions on the best way to set up reliable early warning systems in areas threatened by rapid landslides in shallow unsaturated granular soil covers.

The research is continuing in order to check the validity and repetitiveness of collected data and to deepen the soil response
355    to weather forcing.

## Data availability

The datasets are freely downloadable from https://doi.org/10.5281/zenodo.4281166 (Comegna et al., 2020).

## Author contribution

LC, ED, RG and LO installed the automatic monitoring station and took care about the maintenance of the instruments. LC
360    analyzed the monitored field data. ED and LO analyzed the results of the laboratory infiltration tests to assume a reliable main wetting curve. LC and LP jointly conceived and set up the paper, discussing the issues with the other three authors. RG provided considerations about the role of vegetation. The contributions of the authors are equal.

## Competing interests

The authors declare that they have no conflict of interest.

365

**Acknowledgements**

The Campania Civil Protection Agency is gratefully acknowledged for providing temperature data.

**References**

Chen, P., Mirus, B., Ning, L., and Godt, J.W.: Effect of Hydraulic Hysteresis on Stability of Infinite Slopes under Steady

370   Infiltration, Journal of Geotechnical and Geoenvironmental Engineering, 143(9), doi:10.1061/(ASCE)GT.1943-5606.0001724, 2017.

Chen, P., Ning, L, and Wei, C.: General Scanning Hysteresis Model for Soil–Water Retention Curves, Journal of Geotechnical and Geoenvironmental Engineering, 145(12), doi:10.1061/(ASCE)GT.1943-5606.0002184, 2019.

Comegna, L., Damiano, E., Greco, R., Guida A., Olivares, L., and Picarelli, L.: Effects of the vegetation on the hydrological

375   behavior of a loose pyroclastic deposit, Procedia Environmental Sciences, 19, 922-931, doi:10.1016/j.proenv.2013.06.102, 2013.

Comegna, L., Damiano, E., Greco, R., Guida A., Olivares, L., and Picarelli, L.: Field hydrological monitoring of a sloping shallow pyroclastic deposit, Canadian Geotechnical Journal, 53(7), 1125-1137, doi:10.1139/cgj-2015-0344, 2016a.

Comegna, L., Damiano, E., Greco, R., Guida A., Olivares, L., and Picarelli, L.: Considerations on the Cervinara slope

380   failure, Landslides and Engineered Slopes - Experience, Theory and Practice,  vol. 2, 663-670, doi:10.1201/9781315375007, 2016b.

Comegna, L., Damiano, E., Greco, R., Olivares, L., and Picarelli, L.: Coupled monitoring of soil moisture and suction in pyroclastic air-fall silty soils, Zenodo, doi:10.5281/zenodo.4281166, 2020.

Comegna, L., De Falco, M., Jalayer, F., Picarelli, L., and Santo A.: The role of the precipitation history on landslide

385   triggering in unsaturated pyroclastic soils, Advancing Culture of Living with Landslides, vol. 4, 307-313, doi: 10.1007/978-3-319-53485-5_35, 2017.

Comegna, L., Rianna, G., Lee, S., and Picarelli, L.: Influence of the wetting path on the mechanical response of shallow unsaturated sloping covers, Computers & Geotechnics, 73(3), 164–169, doi:10.1016/j.compgeo.2015.11.026, 2016c.

Damiano, E.: Meccanismi di innesco di colate di fango in terreni piroclastici, PhD Thesis, Università di Roma La Sapienza,

390   2004.

Damiano, E., and Olivares, L.: The role of infiltration processes in steep slope stability of pyroclastic granular soils: laboratory and numerical investigation, Natural Hazards, 52, 329-350, 2010.

Damiano, E., Olivares, L., and Picarelli L.: Steep-slope monitoring in unsaturated pyroclastic soils, Engineering Geology, 137-138, 1-12, 2012.

395   Fiorillo, F., Guadagno, F.M., Aquino, S., and De Blasio, A.: The December 1999 Cervinara landslides: further debris flows in the pyroclastic deposits of Campania (southern Italy), Bulletin of Engineering Geology and the Environment, 60(3), 171–184, doi:10.1007/s100640000093, 2001.

Greco, R., Comegna, L., Damiano, E., Guida, A., Olivares, L. and Picarelli L.: Hydrological modelling of a slope covered with shallow pyroclastic deposits from field monitoring data, Hydrol Earth Syst Sci, 17, 4001–4013, doi:10.5194/hess-17-
400     4001-2013, 2013.

Guadagno, F.M., Revellino, P., and Grelle, G.: The 1998 Sarno landslides: conflicting interpretations of a natural event, Proceedings of the 5th International Conference on Debris-Flow Hazards Mitigation: Mechanics, Prediction and Assessment, Italian Journal of Engineering Geology and Environment, Casa Editrice Universita La Sapienza, url: www.ijege.uniroma1.it. doi:10.4408/IJEGE.2011-03.B-009, 2011.

405     Guida, A., Comegna, L., Damiano, E., Greco, R., Olivares, L., and Picarelli, L: Soil characterization from monitoring over steep slopes in layered granular volcanic deposits, Proceedings of the 2nd Italian Workshop on Landslides, Naples, 28–30 September 2011, Edited by L. Picarelli, R. Greco, and G. Urciuoli, Cooperativa Universitaria Editrice Studi, Fisciano, 147–153, 2012.

Li, XS: Modelling of hysteresis response for arbitrary wetting/drying paths, Computers and Geotechnics, 32, 133-137, 2005.

410     Marino, P., Comegna, L., Damiano, E., Olivares, L., and Greco, R.: Monitoring the hydrological balance of a landslide-prone slope covered by pyroclastic deposits over limestone fractured bedrock, Water, 2020 (submitted for publication).

Mualem, Y.: Hysteretical models for prediction of the hydraulic conductivity of unsaturated porous media, Water Resour Res, 12, 1248-1254, 1976.

Olivares, L., Andreozzi, L., Damiano, E., Avolio, B., and Picarelli, L.: Hydrologic response of a steep slope in unsaturated
415     pyroclastic soils, Proceedings of the International Conference on Fast Slope Movements — Prediction and Prevention for Risk Mitigation, Naples, 11–13 May 2003, Edited by L. Picarelli, Patron Editore, Bologna, Vol. 1, 391–398, 2003.

Olivares, L., Damiano, E., Netti, N., and de Cristofaro, M.: Geotechnical Properties of Two Pyroclastic Deposits Involved in Catastrophic Flowslides for Implementation in Early Warning Systems, Geosciences, 9(1), 24, doi:10.3390/geosciences9010024, 2019.

420     Olivares, L., and Picarelli, L.: Shallow flowslides triggered by intense rainfalls on natural slopes covered by loose un-saturated pyroclastic soils, Geotechnique, 53(2), 283–288, 2003.

Pham, H.Q.: An engineering model of hysteresis for soil–water characteristic curves, MSc thesis University of Saskatchewan, Canada, 2002.

Picarelli, L., Evangelista, A., Rolandi, G., Paone, A., Nicotera, M.V., Olivares, L., Scotto di Santolo, A., Lampitiello, S., and
425     Rolandi, M.: Mechanical properties of pyroclastic soils in Campania Region, Proceedings of the 2nd International Work. on Characterisation and Engineering Properties of Natural Soils, Singapore, Vol. 3, 2331–2383, 2006.

Pirone, M., Papa, R., Nicotera, M.V., and Urciuoli, G.: Evaluation of the hydraulic hysteresis of unsaturated pyroclastic soils by in situ measurements, Procedia Earth and Planetary Sciences, 9, 163-170, 2014.

Rianna, G., Comegna, L., Pagano, L., Picarelli, L., and Reder, A.: The role of hydraulic hysteresis on the hydrological
430     response of pyroclastic silty covers, Water, 11(3), 628, doi:10.3390/w11030628, 2019.

Tami, D., Rahardjo, H., and Leong, E.C.: Effects of hysteresis on steady-state infiltration in unsaturated slopes, J Geotech Geoenviron Eng, 130(9), 956-966, 2004.

Tarantino, A.: A water retention model for deformable soils, Géotechnique, 59(9), 751-762, 2009.

Thornthwaite, C.W.: An approach toward a rational classification of climate, Transactions of the American Geophysical
435   Union, 27(1), 1946.

Topp, G.C., Davis J.L., and Annan A.P.: Electromagnetic determination of soil water content: measurement in coaxial transmission lines, Water Resour. Res., 16, 574-582, 1980.

van Genuchten, M.T.: A closed-form equation for predicting the hydraulic conductivity of unsaturated soils, Soil Sci. Soc. Am. J., 44, 892-898, 1980.

440   Vanapalli, S.K., Fredlund, D.G., Pufahl, D.E., and Clifton AW.: Model for the prediction of shear strength with respect to soil suction, Canadian Geotechnical Journal, 33, 379-392, 1996.

Wheeler, S.J., Sharma, R.S., and Buisson, M.S.R.: Coupling of hydraulic hysteresis and stress–strain behaviour in unsaturated soils, Géotechnique, 53(1), 41-54, 2003.

Yang, C., Sheng, D., and Carter, J.P.: Effect of hydraulic hysteresis on seepage analysis for unsaturated soils, Computers and
445   Geotechnics, 41, 36-56, 2012.